This is the peer-reviewed, final accepted version for American Mineralogist, published by the Mineralogical Society of America.
The published version is subject to change. Cite as Authors (Year) Title. American Mineralogist, in press.
DOI: https://doi.org/10.2138/am-2021-7875. http://www.minsocam.org/

REVISION I

Chemical variability in vyacheslavite, $U(PO_4)(OH)$: crystal-chemical implications for hydrous and hydroxylated U^{4+}, Ca and *REE* phosphates

GWLADYS STECIUK[1], RADEK ŠKODA[2], VERONIKA DILLINGEROVÁ[2,3] AND JAKUB PLÁŠIL[1§]

[1] Institute of Physics ASCR, v.v.i., Na Slovance 1999/2, 18221 Prague 8, Czech Republic

[2] Department of Geological Sciences, Faculty of Science, Masaryk University, Kotlářská 2, 611 37, Brno, Czech Republic

[3] Department of Chemistry, Faculty of Science, Masaryk University, Kotlářská 2, CZ-611 37 Brno, Czech Republic

ABSTRACT

Particularly interesting chemical variability in the U^{4+} phosphate mineral vyacheslavite from Menzenschwand (Germany) has been discovered and investigated by means of electron-diffraction and micro-chemical methods. Suggested variability comprises namely the elevated contents of calcium and rare-earth elements (*REE*s). Based on the crystal structure refinement from 3D electron diffraction data, the structural formula of Ca-rich vyacheslavite studied is $U_{0.895}Ca_{0.105}PO_4(OH)_{0.790}(H_2O)_{0.210}$. In general, such compositional variability involving Ca^{2+} can be expressed as $U_{1-x}Ca_xPO_4(OH)_{1-2x}(H_2O)_{2x}$. Based on detailed electron-probe microanalysis, regions extremely enriched in Y and Ln have been discovered, characterized by the contents up to 11 wt. % of Y_2O_3 and ~4.5 wt. % of Ln_2O_3. In addition to the above-mentioned substitution mechanism, substitution involving Y and *Ln* can be expressed as $U^{4+} + OH^- \rightarrow REE^{3+} + H_2O$. Though the structure refinement has not provided direct evidence of H_2O in the studied nano-fragments of vyacheslavite, the presence of H_2O and its substitution at OH^- sites is a reasonable

§ Email: plasil@fzu.cz

and necessary charge-balancing mechanism. One H atom site was located during structure refinements, however, an additional H-site is only partially occupied and thus was not revealed from the refinement despite of the high-quality data. Substitutional trends observed here suggest possible miscibility or structural relationship between vyacheslavite, rhabdophane and ningyoite that may depend strongly on OH/H_2O content; considering that all crystallize under similar paragenetic conditions.

Keywords: vyacheslavite; crystal structure; chemical composition; electron-diffraction tomography; miscibility, rhabdophane, uranium deposits.

INTRODUCTION

Only two U^{4+} phosphates without additional metal cations are known from nature: lermontovite $U^{4+}(PO_4)(OH)(H_2O)$ (Melkov et al. 1984), and vyacheslavite, $U^{4+}(PO_4)(OH)$ (Belova et al. 1984). These minerals form as products of reduction of U^{6+} to U^{4+} in the supergene enrichment areas of the oxidation zones of U deposits. Togetherwith the other U^{4+}-containing mineral, ningyoite, $CaU^{4+}(PO_4)_2(H_2O)_2$, they are substantial constituents of secondary U deposits and are of considerable economic importance (Doinikova 2007). Nevertheless, they have remained poorly defined, due to the fact that they are usually poorly crystalline or only form nanocrystals, preventing them from being characterized by conventional methods. Recently, Steciuk et al. (2019) reported the first structure determination of vyacheslavite from natural nanocrystals using 3D electron diffraction technique (Vincent and Midgley 1994; Gemmi and Lanza 2019; Gemmi and Mugniaoli 2019). Additionally, Density-Functional-Theory (DFT) calculations (Steciuk et al. 2019) showed that vyacheslavite contains no molecular H_2O, in contrast to previous findings

(Belova et al. 1984). During crystal structure studies, we observed significant chemical variability in specimens of vyacheslavite originating from the Menzenschwand uranium deposit (Black Forest Mts., Germany). Here, we report on the results of this study, documenting that (Ca,*REE*)-rich vyacheslavite may represent an intermediate partially hydrated member related to U^{4+}, Ca^{2+}, Ln^{3+}-bearing hydroxyl phosphates, such as ningyoite and rhabdophane.

MATERIAL DESCRIPTION

Samples we investigated in this study originate from the Menzenschwand (Krunkelbach) uranium deposit, Black Forest Mountains, Germany, and were retrieved from the former Dietre Nicolai collection via Carsten Slotta (Mintreasure.com). The matrix of the specimen consists of quartz (partially smoky-quartz), which crystallized into cavities. The pyramidal terminations of quartz are covered by limonite overgrown by dark-green to the green crusts of vyacheslavite. Abundant hematite is also present. Crusts of vyacheslavite revealed upon trimming cover primary ore minerals, which have a metallic or semi-metallic luster. Uraninite and pyrite occur intimately associated.

CHEMICAL ANALYSIS

Vyacheslavite and related minerals were analyzed by electron microprobe using a Cameca SX100 electron microprobe (Masaryk University, Brno) operating in wavelength dispersive spectroscopy mode using an accelerating voltage of 15 kV, and a beam current of 20 nA for vyacheslavite and 40 nA for uraninite. The beam diameter was set to 15 μm for vyacheslavite and 5 μm for (Ca*, REE*)-rich vyacheslavite and uraninite. Concentrations of elements other than those reported in Table 1 were below detection limits (ca 0.05–0.10 wt. %). Standards used for

72 calibration are listed in Table 1. Raw X-ray intensities were corrected for matrix effects with a
73 $\phi(\rho z)$ algorithm of *X-PHI* routine (Merlet 1994).

74 Uraninite was measured using prolonged counting times on Pb *M*α (240s), and on U *M*β,
75 Th *M*α and Y *L*α (60s) in order to improve the statistics for chemical dating. Additionally, the
76 concentration of Pb and U were corrected for spectral interferences, see Škácha et al. (2009) for
77 details. Assuming that the total Pb in uraninite is radiogenic, the chemical age was calculated by
78 the equation published by Montel et al. (1996).

79

80 *Laser ablation-ion-coupled-plasma mass spectroscopy (LA-ICP-MS)*

81 The trace-element content of vyacheslavite and uraninite was investigated by LA-ICP-MS
82 using an Agilent 7500ce quadrupole ICP-MS with an attached UP 213 laser ablation system. The
83 sample was ablated using a Q-switched Nd:YAG laser operating at a wavelength of 213 nm
84 (pulse duration of 4.2 ns). Ablated material was transported from the sample chamber using
85 helium carrier gas (1 L/min) and mixed with argon (0.6 L/min) prior to the torch. Potential
86 polyatomic interferences were minimized by a collision reaction cell in He mode (2 mL/min).
87 The contents of major to trace elements were determined after laser ablation of individual spots at
88 the following conditions: diameter 55 μm, fluence of laser beam 7 $J.cm^{-2}$, frequency 10 Hz and
89 spot ablation time 60 s. The contents of elements of interest were determined using SRM NIST
90 610 as a standard, NIST 612 as an internal control and U and Ca as an internal reference element.
91 Calculations were performed after baseline correction and integration of peak areas.

92

93 *Vyacheslavite*

Vyacheslavite is, along with uraninite, a dominant component of the studied section (Fig. 1). Locally grains of clausthalite, PbSe, are sparsely embedded. In general, vyacheslavite is chemically homogeneous in BSE images, except of very narrow rims at the border with uraninite grains which are darker, qualitatively, possibly due to less enrichment in *REE*s or higher Ca:U content. These rims adhere to a (Ca, *REE*)-rich vyacheslavite (see below). Typical vyacheslavite, nevertheless, also contains *Ln* and Y, up to ~1.5 wt. % Ln_2O_3 and ~ 3 wt. % Y_2O_3 and a slightly elevated content of Ca (~0.8 wt. % CaO). Elemental maps in Fig. 2 demonstrate the chemical variability and textural relations among these phases. The occupancy of the octahedral site of vyacheslavite is shown in Fig. 6. The sum of the analyzed oxides is ~96.5 wt. %. The corresponding empirical formula calculated from 9 individual analyses on the basis of 2 cations *pfu* is: $U_{0.87}Ca_{0.05}Y_{0.08}Ln_{0.02}[(PO_4)_{0.80}(SiO_4)_{0.10}(AsO_4)_{0.05}(AlO_4)_{0.02}(SO_4)_{0.01}](OH)_{0.87}$ The sum of *Ln*, determined by LA-ICP-MS, is ~14000 ppm, where the dominant Ln^{3+} is Dy, at ~3500 ppm, see Table 2). The *REE* pattern normalized to post-Archean Australian Shale (PAAS, McLennan, 1989) shows a strong depletion in light *REE* and only a small Eu anomaly ($Eu_N/Eu^*_N = 1.57$), see Fig. 4.

(Ca, REE)-rich vyacheslavite

In the polished-section studied, (Ca, *REE*)-rich vyacheslavite has been identified forming thin (~5 μm) rims and isolated aggregates at the border with uraninite. From observations in BSE images (Fig. 1, 2), it is also apparent that locally, this rim issurrounded by a thin "crust" of uraninite. In places, uraninite forms isolated globular aggregates in vyacheslavite. This type of vyacheslavite is characteristic by increased contents of Y (up to 11 wt. % of Y_2O_3), Ln (~4.5 wt. % of Ln_2O_3), and Ca (3.8 wt. % CaO). It also contains less As but more Si (Table 1) than

vyacheslavite, which is more distant from uraninite. The empirical formula calculated from 3 individual analyses on the basis of 2 cations *pfu* is: $U_{0.64}Y_{0.29}Ca_{0.20}Ln_{0.07}[(PO_4)_{0.66}(SiO_4)_{0.11}(AsO_4)_{0.02}(AlO_4)_{0.01}](OH)_{1.47}$ (where the dominant Ln^{3+} is Dy). The small size of this phase did not allow trace-element measurements for the suite of *Ln* by LA-ICP-MS. The occupancy of the octahedral site based on these analyses is shown in Fig. 3.

Uraninite

Uraninite is a mixed-valence uranium oxide with a defective fluorite-type structure, which can accommodate a large amount of di- and trivalent elements (Ca^{2+}, REE^{3+}), and thus the structural formula can be expressed as $(U^{4+}_{1-x-y-z}U^{6+}_{x}R^{3+}_{y}R^{2+}_{z})O_{2+x-0.5y-z}$ (Janeczek and Ewing 1992). The presence of Si in uraninite analyses is typically ascribed to coffinitization; however, a high content of V, As, P, and Zr has been occasionally reported (Škácha et al. 2009, Alexandre et al. 2015, René et al. 2019). Usually, high P, As or Zr content is concurrent with elevated Si content.

Uraninite aggregates associated with vyacheslavite are homogeneous in BSE images, lacking apparent features of alteration (besides replacement by vyacheslavite along the rim) and encloses pyrite fragments in the central parts. The chemical composition of uraninite is characterized by high As content (3.9 wt. % of As_2O_5) and P (2.3 wt. % of P_2O_5) and an elevated content of Ca (0.3 wt. % CaO), Al (0.5 wt. % of Al_2O_3) and Y (0.2 wt. % of Y_2O_3) and remarkably low Si (0.3 wt. % SiO_2), see Table 1. Considering U as tetravalent, the total is 97.4 wt. %; the presence of U^{6+}, which was not measured but is very likely present,would led to slightly higher calculated totals. Low chemical variability and limited number of analyses do not allow for an elucidation of the substitution mechanisms involving As and P into the uraninite structure. The content of *Ln* s in uraninite obtained from LA-ICP-MS is ~2000 ppm again,

containing Dy as the most abundant element (Table 2). Distribution of *REE* normalized by Post Archean Australian Shale (PAAS; McLennan 1989) and its comparison with the *REE* pattern of uraninite I–III form Menzeschwand (Göb et al. 2013) is shown in Fig. 4. Concerning uraninite II and III (Göb et al. 2013), uraninite associated with vyacheslavite is lean in light *REE* and enriched in medium to heavy *REE*. The shape of the *REE* pattern of studied uraninite, vyacheslavite, and (Ca, *REE*)-rich vyacheslavite are similar, but the latter phase has several times higher *REE* content with respect to uraninite (*c.f.*, Fig. 4).

STRUCTURE OF CA-RICH VYACHESLAVITE

Single-crystal 3D electron diffraction

For transmission electron microscopy (TEM) investigations, the sample was crushed without solvent and deposited on a Cu-grid with a thin film of holey amorphous carbon. The grid was plunged into liquid nitrogen and then transferred to a FEI Tecnai 02 transmission electron microscope (TEM) (acceleration voltage of 200 kV, LaB_6) using a Gatan cryo-transfer holder. Precession-assisted 3D electron diffraction (3D ED) data sets of non-oriented patterns (see Vincent and Midgley 1994; Kolb et al. 2007, 2008; Gemmi et al. 2019) were recorded at 100K on several crystals with the precession device Nanomegas Digistar and a side-mounted CCD camera Olympus Veleta with 14bit dynamic range energy-dispersive analyzer Octane silicon drift detector (SDD) EDAX (Fig. 5). The precession angle was set to 1° with a tilt step of 1°. To preserve the crystal during the data acquisiton, low illumination setting were used (condenser aperture of 10 μm with a spot size 7 or 8 μm). 3D ED data were analyzed using the computer programs PETS2.0 (Palatinus et al. 2019), Superflip (Palatinus and Chapuis 2007), and Jana2006 (Petříček et al. 2014). For each 3D ED data set, two *hkl*-type files are obtained with associated

intensities and estimated standard deviations based on counting statistics: one for structure solution and the kinematical refinement, and another file dedicated to the dynamical refinement where each ED frame is considered independent (Palatinus et al. 2015a, b). We focused our attention on the Ca-rich areas of vyacheslavite that can be easily located *via* EDS coupled to our TEM.

Data processing and refinement

All the data sets were processed using the new options available in PETS2.0: especially the optimization of the frame orientation that improves data reduction and refinement. The refinement of Ca-rich vyacheslavite was first performed without the hydrogen position to determine the proportion of calcium (Fig. 6). All refinements have been done using Jana2006.

The refinement against the four 3D ED data sets independently gives a Ca proportion ranging from 0.057(7) to 0.123(5) Ca, and the combination of all data leads to Ca = 0.104(3). These refinements were carried out, assuming only Ca and U in the site. Refinements with and without Ca substituting for U provided similar R_{obs} values: R_{obs} (without Ca) = 0.0919, R_{obs} (with Ca) = 0.0910 (Table 3). However, the values of atomic displacement parameters decreased significantly to reach a more relevant value. The presence of a maximum corresponding to the expected hydrogen position in the difference electrostatic potential map is an indication of the high data quality (Fig. 6). As the next step, refinement, including hydrogen, was done by combining all four data blocks in order to improve the statistics. Yttrium was not considered in the refinement as it was not relevant to introduce a third atom (Y) having a scattering power between Ca and U. It means that the refined amount of Ca is most likely overestimated in this study. However, the evolution of the atomic displacement parameter for the U site after

186 introduction of Ca clearly indicates the presence of atom with a lower-scattering power than that
187 of U (meaning those of Ca+Y).
188
189 *Structure description*
190 Generally, the structure of Ca-rich vyacheslavite is similar to that of vyacheslavite
191 reported already (Steciuk et al. 2019). It contains a U^{4+} cation coordinated in the form of a
192 distorted square antiprism. The U polyhedra share edges with PO_4 tetrahedra to form chains
193 extending parallel to [100]. The chains polymerize along the [010] by sharing edges between U
194 polyhedra, and by U polyhedra sharing corners with the PO_4 tetrahedra of the adjacent chains.
195 The structure thus contains complex uranium phosphate sheets running parallel to (001). These
196 are interlinked by PO_4 tetrahedra that share corners with U polyhedra from the next layer. The
197 result is a robust framework with cavities.
198 In the case of the Ca-rich vyacheslavite the strongest residual electrostatic potential
199 maxima obtained after inclusion of the H atom into the refinement is most likely a Fourier-series
200 artifact stemming from the symmetry. After several tests, we concluded that it cannot correspond
201 to any additional oxygen position present instead of the O4 atom when the U is substituted by Ca.
202 The first attempts showed that it is not compatible with reasonable bond valence values
203 calculated then for Ca (>3.5 *vu*). Moreover, it led to negative ADPs for this additional O site.
204 The final structural parameters for the Ca-rich vyacheslavite can be found in the CIF file
205 given as supplementary. The refined structure model is displayed in Fig. 6; refinement parameters
206 are listed in Table 3. With an average *x* value of 0.105, the composition can be written as
207 $U_{0.895}Ca_{0.105}PO_4(OH)_{0.790}(H_2O)_{0.210}$ (assuming no Y). The bond-valence analysis supports the

assumption that locally, H_2O substitutes for OH^- in the structure to compensate for $Ca^{2+}U^{4+}_{-1}$ substitution (Table 3).

DISCUSSION

Ca^{2+} and REE^{3+} for U^{4+} substitution mechanism

When U^{4+} is substituted by Ca^{2+}, two positive charges have to be compensated to keep the structure electroneutral. The first option would comprise a partially occupied O4 (and corresponding H1o4) as $(OH)_{1-2x}$ (where x is the Ca-fraction). Nevertheless, it is not likely, namely, because the hydrogen position was evident from the difference Fourier map, it is likely then that it cannot correspond just to a partially occupied H site. The second option to be considered: an H_2O instead of the OH is present when the Ca substitution takes place, leading to an aqua-hydroxo calcium complex. Therefore, the vyacheslavite composition as studied by electron diffraction, may be expressed as $U_{1-x}Ca_xPO_4(OH)_{1-2x}(H_2O)_{2x}$. The conclusion is that the additional H-site is only partially occupied, possibly disordered and cannot be thus revealed from the refinement despite the high-quality data. The electron-probe microanalysis, nevertheless, documented high concentrations of REE^{3+} along with Ca^{2+}, at least at some regions of the studied section. Similarly, to the substitution of Ca^{2+} for U^{4+} as $U^{4+} + 2OH^- \rightarrow Ca^{2+} + 2H_2O$, the substitution involving Y and *Ln* can be simply given as $U^{4+} + OH^- \rightarrow REE^{3+} + H_2O$.

Structure implications for ningyoite

Ningyoite has been described by Muto et al. (1959) as the main ore mineral in exogenic U deposits near Ningyo-Toge, Japan. They ascribed to it the formula $U_{1-x}Ca_{1-x}REE_{2x}(PO_4)_2(H_2O)_{1-2}$, where x ranges from ~0.1 to 0.2. Later on (see, e.g., Doinikova 2007), the formula was

231 expressed in a simplified form, $CaU(PO_4)_2 \cdot 2H_2O$. The official IMA formula kept today is
232 $(U,Ca,Ce)_2(PO_4)_2 \cdot 1–2H_2O$. The structure of this mineral has not been solved so far. Nevertheless,
233 Muto et al. (1959) based on the similarity of the ningyoite powder XRD data and rhabdophane,
234 concluded that ningyoite has a rhabdophane-type structure and possibly can form a solid solution.
235 Based on current work it is impossible to decide if ningyoite adopts the rhabdophane- or
236 vyacheslavite-type structure. The close chemical relationship of these minerals with churchite-
237 (Y), and its potential connection with other Ca, U^{4+}, REE-phosphate mineral equilibria cannot be
238 ignored, although it adopts an entirely distinctive crystal structure (Kohlman et al. 1994).
239 Notwithstanding, both the structural and WDS investigations led us to the hypothesis that a solid-
240 solution or at least a close topological similarity may exist between vyacheslavite and ningyoite
241 (Fig. 4). Its extent is dependent on the capability of the vyacheslavite structure to accommodate
242 H_2O. On close inspection of the structure of rhabdophane-(Ce) (Money 1948), we can distinguish
243 certain significant differences, namely in the connectivity between Ce and PO_4 in rhabdophane
244 and U/Ca and PO_4 in vyacheslavite (Fig. 6). In summary, the accommodation of *REE* and Ca,
245 along with H_2O incorporationdue to the charge-balance requirements into the vyacheslavite
246 structure is possible, but the extent remains unknown as well as the answer to the question of
247 whether ningyoite has a rhabdophane-type of structure or it is just somewhat similar. These
248 questions remain open for future research.

249 Chemical analyses of natural ningyoite commonly show enrichment in *REE*, *via* the
250 substitution $Ca^{2+} + U^{4+} \rightarrow 2REE^{3+}$ and a departure from the ideal stoichiometry in the octahedral
251 site, as well as between octahedral and tetrahedral sites, and commonly contains elevated
252 amounts of Fe, Pb (common), Zr, Si, and S (Scharmova and Scharm 1994; René et al. 2019). The
253 tetrahedral-site deficiency also observed in the (Ca, *REE*)-rich vyacheslavite from

Menzenschwand and elevated Si, Fe and S supports that the observed compositional variation trends towards a substantial chemical similarity with ningyoite.

Based on the high Ca and P content in coffinite, $U^{4+}SiO_4(H_2O)_n$, $0< n <2$ (Deditius et al. 2008), from Bangombé, Gabon, Janeczek and Ewing (1996) suggested a solid solution between coffinite and ningyoite. However, TEM observations of similar phases from the same locality instead revealed xenotime-type substitution and nanoscale intergrowths of amorphous coffinite and (U, Ca, *REE*) phosphate (Utsunomiya et al. 2008, Deditius et al. 2009). Considering these observations, we are unable to conclude whether elevated Si contents in vyacheslavite and (Ca, *REE*)-rich vyacheslavite could represent participation of the coffinite-moiety *via* a different substitution vector, or whether it represents a nanoscale intergrowths with the Si-rich phase.

Vyacheslavite occurrence at Menzenschwand: conditions of formation

The Menzenschwand U deposit in the Black Forest Mts. (Baden-Würtemberg, Germany), is famous for various supergene uranium minerals; the zone of the supergene oxidation is extensively developed (Markl and Wolfsried 2011). Among the known supergene U minerals that occur there, two contain U in the reduced form: vyacheslavite and the uranyl-oxide mineral ianthinite, $[U^{4+}{}_2(UO_2)_4O_6(OH)_4(H_2O)_4](H_2O)_5$ (Burns et al. 1997). Both minerals occur in a somewhat similar association, which is, however, relatively common at Menzenschwand. In the quartz gangue there is abundant fluorite, hematite, and sulfides, and among others, unusually large amounts of pyrite. The significant role of pyrite (and other sulfides) and its oxidation has been stressed by Göb et al. (2013). The presence of both vyacheslavite and ianthinite is tightly linked either to the relative abundance of pyrite (and uraninite) in the gangue or to the abundance of goethite and other Fe-supergene oxidemechanismplausible for the formation of vyacheslavite

in the corresponding step no. 3: "If the reaction with sulfide proceeds, it can lead to a significant decrease of f_{O2} and finally to the reduction of U^{6+} to U^{4+} and precipitation of uraninite. The observed pseudomorphs of uraninite III after secondary uranyl minerals (especially ianthinite) or pyrite are nicely explained by this scenario, which would occur if water percolating through the rock gets trapped in a vug and reacts under the closed-system conditions and low-fluid/mineral ratios with the sulfides in direct contact." The vuggy (cavernous) quartz gangue seems to be an ideal trap, where such micro-conditions can develop. For the formation of vyacheslavite, the presence of PO_4^{3-} is necessary to be within the system. As noted by Göb et al. (2013), phosphate minerals are abundant in Menzenschwand in general. However, phosphate concentrations in the (recent) mining waters are low (Göb et al. 2013), which can be explained by the effective removal of phosphate from the Menzenschwand waters, most probably by precipitation of phosphates. They further claimed that the hypothesis is further supported by the fact that, besides uranyl phosphates,other phosphates are common at Menzenschwand, namely the *REE*-phosphate churchite-(Y) and the Ba-Al phosphate gorceixite (Hofmann 1989; Göb et al. 2011, 2013; Markl and Wolfsried 2011). Nevertheless, it is very likely that phosphate necessary for the formation of vyacheslavite originates from the dissolution of torbernite as the pH of the solution decreases by the continuing massive pyrite oxidation (*c.f.* step I *in* Göb et al. 2013). Phosphorus, can be, however, also derived from the dissolution of apatite (e.g in the host rock), which is unstable under the low pH.

Based on SEM/BSE observations, it is likely that vyacheslavite replaces uraninite *in-situ*, forming pseudomorphoses that adopt the colomorph texture of the original pitchblende (Fig. 1), or that it assumed this shape by growing along the surfaces of uraninite grains. The *REE* patterns of vyacheslavite and pitchblende are very similar (Fig. 4); the only difference is the magnitude of

300 *REE* concentration, which is much higher in vyacheslavite, *i.e.,* in the product of the reaction. It
301 seems that little to no *REE* fractionation takes place during its formation, as there is no or only
302 weak positive anomaly in Ce content. We think this supports the scenario mentioned above (step
303 #3 in Göb et al. 2013), which comprises local andisolated systems. While the phosphate was
304 obtained from locally dissolved torbernite, U could be derived both from torbernite and uraninite
305 and *REE* is unambiguously sourced from altered uraninite. We note that normalized *REE* pattern
306 of vyacheslavite from Menzenschwand is entirely distinct from those reported for uranyl silicates
307 by Göb et al. (2013), but similar to uranyl phosphates and arsenates as well as the waters sampled
308 in mine (Göb et al. 2013), that differ in the magnitude of concentration. This can, however,
309 suggest that it formed from the same fluids percolating at Menzenschwand (and from uranyl
310 phosphates and arsenates formed there, in general). This is in line with the conclusion of Göb et
311 al. (2013): "Their *REE* patterns reflect those of the host-rock derived waters (Fig. 7), which
312 suggests input from the host rock. However, since fluorite from the vein has an *REE* pattern
313 similar to those observed in the uranyl phosphates and arsenates, an influence from the vein is
314 also possible." It is possible that both mechanisms contributed (depending on localconditions) to
315 vyacheslavite formation.
316
317 *Chemical dating of uraninite*
318 The Menzenschwand deposit is located at the vicinity of the Krunkelbach fault in Bärhalde
319 granite (14 ppm U; Hofmann and Eikenberg 1991), which hosts magmatic uraninite (uraninite I
320 following the terminology by Göb et al. 2013) which is believed to be a source of hydrothermal
321 uraninite (uraninite II) of Menzenschwand deposit. Its formation was dated to roughly 300 Ma by
322 various isotopic techniques (Hofmann and Eikenberg 1991; Meshik et al. 2000) with a lower

limit U–Pb uraninite II discordia intersection at ca. 50 Ma, indicating the age of Pb-loss. Hoffmann and Eikenberg (1991) also reported chemical ages of uraninite in the range 41–49 Ma, which agree reasonably well with the discordia intersection age, indicating it was likely formed during tertiary hydrothermal activity. Various secondary uranium minerals were dated between roughly 0.3–1.75 Ma (Hoffmann and Eikenberg 1991; Pfaff et al. 2009). Electron microprobe chemical dating of uraninite associated with vyacheslavite yields a consistent age of 18 ±4 Ma (*n* = 5). This is significantly lower than has been reported by Hoffmann and Eikenberg (1991). The uraninite studied here is typically enriched in As_2O_5 (3.9 wt. %), P_2O_5 (2.3 wt. %) with low SiO_2 and CaO content. Such composition differs from eight morphological and genetic types of uraninite analyzed by Hoffmann and Eikenberg (1991). The *REE* content and pattern of this uraninite differ from uraninite I–III published by Göb et al. (2013), both in the shape of the normalized pattern andin character of the Eu anomaly. Göb et al. (2013) used the plot of Gd_N/Lu_N vs La_N/Gd_N ratios to discriminate uraninite I–III generations, reproduced here in Fig. 7. Uraninite associated with vyacheslavite does not fall into the uraninite I and II fields, and is distinct from the two analyses of uraninite III. Thus, the uraninite associated with Ca-rich vyacheslavite may represent a separate generation formed by later hydrothermal Miocene event at 18 Ma. As there is no isotopic control in the chemical dating method, it might also represent an older uraninite reworked during a hydrothermal event which caused a Pb loss. If we follow this scenario, the consistent age of individual uraninite analyses (SD = 1.4) could indicate a complete age resetting during the hydrothermal even at 18 Ma.

There were no inclusions of Pb-rich phases within uraninite, which would provide evidence for the remobilization of radiogenic lead. On the other hand, the Pb-selenide mineral clausthalite occurs as small inclusions within vyacheslavite, spatially related to the contact with

346 uraninite. Their formation during uraninite replacement by vyacheslavite is likely because the
347 vyacheslavite structure obviously does not prefer the incorporation of Pb. Its content in
348 vyacheslavite is below the DL of electron microprobe (<0.10 wt. % Pb). Co-precipitation of
349 clausthalite and vyacheslavite is in accordance with reducing conditions necessary for the
350 formation of both phases.

351 ## IMPLICATIONS

352 Though vyacheslavite had been documented to be anhydrous, i.e. $U(PO_4)(OH)$, our current study
353 has indicated this phase exhibits more significant chemical variability, manifested namely by the
354 incirporation of Ca^{2+} and REE^{3+}. This variability is connected with the substitution of H_2O for
355 OH, necessary for charge balance. Such substitution plays an important role in the formation of
356 (and substitutions of) related uranyl oxysalts formed under low pT conditions.

357 Interestingly, vyacheslavite does not accumulate Pb, despite the fact that in the currently
358 investigated system lead is abundant – manifested by the presence of clausthalite, PbSe. In
359 general, both ningyoite and rhabdophane accommodate higher amounts of Pb, much higher than
360 the amount of radiogenic Pb formed from U-decay. The reason why is, unfortunately, beyond the
361 scope of this study. Nevertheless, we found it particularly interesting and useful for radiometric
362 dating.

363 ## ACKNOWLEDGEMENTS

364 We would like to express our thanks to Stephan Wolfsried (Waiblingen, Germany) and
365 Carsten Slotta (Hausach, Germany) for their kind cooperation in providing us with the specimens
366 used in this research project. The earlier version of the manuscript greatly benefited from the

constructive reviews of an anonymous referee and Travis Olds. This study was funded by the Czech Science Foundation (GACR 20-11949S to GS and JP), and by OP VVV project (Geobarr CZ.02.1.01/0.0/0.0/16_026/0008459 to RS).

REFERENCES

Alexandre, P., Kyser, K., Layton-Matthews, D., Joy, B. and Uvarova, Y. (2015) Chemical compositions of natural uraninite. Canadian Mineralogist, 53(4), 595–622.

Belova, L.N., Gorshkov, A.I., Ivanova, O.A., Sivtsov, A.V., Lizorkina, L.I. and Voronikhin, V.A. (1984) Vyacheslavite $U^{4+}(PO_4)(OH)\cdot nH_2O$ - a new uranium phosphate. Zapiski Vsesoyuznogo Mineralogicheskogo Obshchestva, 113(3), 360–365.

Burns, P.C., Finch, R.J., Hawthorne, F.C., Miller, M.L. and Ewing, R.C. (1997) The crystal structure of ianthinite, $[U^{4+}{}_2(UO_2)_4O_6(OH)_4(H_2O)_4](H_2O)_5$: a possible phase for Pu^{4+} incorporation during the oxidation of spent nuclear fuel. Journal of Nuclear Materials, 249, 199–206.

Deditius, A. P., Utsunomiya, S. and Ewing, R. C. (2008) The chemical stability of coffinite, $USiO_4\cdot nH_2O$; $0 < n < 2$, associated with organic matter: A case study from Grants uranium region, New Mexico, USA. Chemical Geology, 251, 33–49.

Deditius, A. P., Utsunomiya, S., Wall, M. A., Pointeau, V. and Ewing, R. C. (2009) Crystal chemistry and radiation-induced amorphization of P-coffinite from the natural fission reactor at Bangombé, Gabon. American Mineralogist, 94, 827–837.

Doinikova, O.A. (2007) Uranium Deposits with a New Phosphate Type of Blacks. Geology of Ore Deposits, 49(1), 80–86.

Gagné, O.C. and Hawthorne, F.C (2015) Comprehensive derivation of bond-valence parameters for ion pairs involving oxygen. Acta Crystallographica, B71, 562–578.

390 Gemmi, M. and Lanza, A.E. (2019) 3D electron diffraction techniques. Acta Crystallographica,
391 B75, 495–504.
392 Gemmi, M., Mugnaioli, E., Gorelik, T.E., Kolb, U., Palatinus, L., Boullay, P., Hovmöller, S. and
393 Abrahams, J.P. (2019) 3D Electron Diffraction: The Nanocrystallography Revolution. ACS
394 Central Science, 5, 1315–1329.
395 Göb, S., Wenzel, T., Bau, M., Jacob, D.E., Loges, A. and Markl, G. (2011) The redistribution of
396 rare-earth elements in secondary minerals of hydrothermal veins, Schwarzwald, southwestern
397 Germany. Canadian Mineralogist, 49, 1305–1333.
398 Göb, S., Guhring, J.E., Bau, M. and Markl, G. (2013) Remobilization of U and *REE* and the
399 formation of secondary minerals in oxidized U deposits. American Mineralogist, 98, 530–
400 548.
401 Hofmann, B. (1989) Genese, Alteration und rezentes Fliess-System der Uranlagerstätte
402 Krunkelbach (Menzenschwand, Südschwarzwald), 195 p. Dissertation, Universität Bern,
403 Switzerland.
404 Hofmann, B. and Eikenberg, J. (1991) The Krunkelbach uranium deposit, Schwarzwald,
405 Germany; correlation of radiometric ages (U–Pb, U–Xe–Kr, K–Ar, ^{230}Th–^{234}U). Economic
406 Geology, 86(5), 1031–1049.
407 Janeczek, J. and Ewing, R. C. (1992) Structural formula of uraninite. Journal of Nuclear
408 Materials, 190, 128–132.
409 Janeczek, J. and Ewing, R. C. (1996) Phosphatian coffinite with rare earth elements and Ce-rich
410 françoisite-(Nd) from sandstone beneath a natural fission reactor at Bangombé, Gabon.
411 Mineralogical Magazine, 60, 665–669.

412 Kohlmann, M., Sowa, H., Reithmeyer, K., Schulz, H., Krüger, R.-R. and Abriel, W. (1994)
413 Structure of a $Y_{1-x}(Gd,Dy,Er)_xPO_4.2H_2O$ microcrystal using synchrotron radiation. Acta
414 Crystallographica C, 50, 1651–1652.
415 McLennan, S.M. (1989) Rare earth elements in sedimentary rocks: Influence of provenance and
416 sedimentary processes. In B.R. Lipin and G.A. McKay, Eds., Geochemistry and Mineralogy
417 of Rare Earth Elements, 21, 169–200. Reviews in Mineralogy, Mineralogical Society of
418 America, Chantilly, Virginia.
419 Markl, G. and Wolfsried, S. (2011) Das Uran von Menzenschwand, 143 p. Christian Weise
420 Verlag München.
421 Melkov, V.G., Belova, L.N., Gorshkov, A.I., Ivanova, O.A., Sivtsov, V.A. and Boronnikhin,
422 V.A. (1983) New data on lermontovite. Mineralogiceskij Zhurnal, 5, 82–87.
423 Merlet, C. (1994) An accurate computer correction program for quantitative electron probe
424 microanalysis. Microchimica Acta, 114/115, 363–376.
425 Meshik, A. P., Lippolt, H. J. and Dymkov, Y. M. (2000) Xenon geochronology of Schwarzwald
426 pitchblendes. Mineralium Deposita, 35, 190–205.
427 Mooney, R. C. L. (1950) X-ray diffraction study of cerous phosphate and related crystals. I.
428 Hexagonal modification. Acta Crystallographica, 3, 337–340.
429 Jean-Marc Montel, S. F., Veschambre, M. and Nicollet, C. (1996) Electron microprobe dating of
430 monazite. Chemical Geology, 131, 37–53.
431 Palatinus, L. and Chapuis, G. (2007) SUPERFLIP – a computer program for the solution of
432 crystal structures by charge flipping in arbitrary dimensions. Journal of Applied
433 Crystallography, 40, 786–790.

Palatinus, L., Petříček, V. and Corrêa, C.A. (2015a) Structure refinement using precession electron diffraction tomography and dynamical diffraction: theory and implementation. Acta Crystallographica, A71, 235–244.

Palatinus, L., Corrêa, C.A., Steciuk, G., Jacob, D., Roussel, P., Boullay, P., Klementová, M., Gemmi, M., Kopeček, J., Domeneghetti, M.Ch., Cámara, F. and Petříček, V. (2015b) Structure refinement using precession electron diffraction tomography and dynamical diffraction: tests on experimental data. Acta Crystallographica, B71, 740–751.

Palatinus, L., Brázda, P., Jelínek, M., Hrdá, J., Steciuk, G. and Klementová, M. (2019) Specifics of the data processing of precession electron diffraction tomography data and their implementation in the program PETS2.0. Acta Crystallographica, B75, 512–522.

Petříček, V., Dušek, M. and Palatinus, L. (2014) Crystallographic Computing System Jana 2006: general features. Zeitschrift für Kristallographie, 229, 345–352.

Pfaff, K., Romer, R. L. and Markl, G. (2009) U–Pb ages of ferberite, chalcedony, agate,'U-mica'and pitchblende: constraints on the mineralization history of the Schwarzwald ore district. European Journal of Mineralogy, 21, 817–836.

René, M., Dolníček, Z., Sejkora, J., Škácha, P. and Šrein, V. (2019) Uraninite, Coffinite and Ninöyoite from Vein-Type Uranium Deposits of the Bohemian Massif (Central European Variscan Belt). Minerals, 9(2), 123.

Scharmová, M. and Scharm, B. (1994) Rhabdophane group minerals in the uranium ore district of northern Bohemia (Czech Republic). Journal of the Czech Geological Society, 39, 267.

Steciuk, G., Ghazisaeed, S., Kiefer, B. and Plášil, J. (2019) Crystal structure of vyacheslavite, $U(PO_4)(OH)$, solved from natural nanocrystal: a precession electron diffraction tomography (PEDT) study and DFT calculations. RSC Advances, 9, 19657–19661.

457 Škácha, P., Goliáš, V., Sejkora, J., Plášil, J., Strnad, L., Škoda, R. and Ježek, J. (2009)
458 Hydrothermal uranium-base metal mineralization of the Jánská vein, Březové Hory, Příbram,
459 Czech Republic: lead isotopes and chemical dating of uraninite. Journal of Geosciences,
460 54(1), 15–56.
461 Utsunomiya, S., Deditius, A. P., Pointeau, V. and Ewing, R. C. (2008) Coffinite and ningyoite
462 from the natural nuclear reactor at Bangombe, Gabon. Geochimica et Cosmochimica Acta,
463 72, A968.
464 Vincent, R. and Midgley, P.A. (1994) Double conical beam-rocking system for measurement of
465 integrated electron diffraction intensities. Ultramicroscopy, 53, 271–282.
466

467

468 FIGURE CAPTIONS

469 **Figure 1.** BSE image of the studied part of polished section containing vyacheslavite, Ca-*REE*-
470 rich vyacheslavite and associated minerals.

471 **Figure 2**. X-ray (WDS) maps of the elemental distribution within the part of the analyzed section
472 (see Fig. 1).

473 **Figure 3.** Ternary plot showing the occupancy of the octahedral site of vyacheslavite and (Ca,
474 *REE*)-rich vyacheslavite form Menzenschwand.

475 **Figure 4.** *REE* patterns of vyacheslavite, (Ca, *REE*)-rich vyacheslavite, and associated uraninite
476 normalized by PAAS (McLennan 1989). For comparison uraninite I-III (Göb et al. 2013) are
477 shown: uraninite I represents magmatic uraninite from Bärhalde granite; uraninite II-
478 hydrothermal uraninite, var. pitchblende; uraninite III, late uraninite replacing ianthinite.

479 **Figure 5**. Crystals used for the 3D ED experiments and the refinements.

480 **Figure 6**. **a)** Projection along the **a**-axis of vyacheslavite structure with a superimposed
481 difference potential map showing maxima at the position of the hydrogen atom (H1o4).
482 Isosurface levels are $3\sigma[\Delta V(r)]$ (orange) and $2\sigma[\Delta V(r)]$ (grey). The difference potential map is
483 obtained after the dynamical refinement using the combination of four 3D ED data sets. The
484 maxima surrounded in green at position (0, 0.5, 0.5) corresponds to a symmetry artifact. **b)**
485 Crystal structure of rhabdophane (after Mooney 1950) viewed down **a**.

Figure 7. Discrimination plot for uraninite and secondary uranium minerals from Menzenschwand adopted from Göb et al. (2013) based on La, Gd and Lu values normalized to PAAS (McLennan1989).

Tables

Table 1. Electron-probe microanalyses (WDS) of vyacheslavite, (Ca,*REE*)-rich vyacheslavite, and uraninite from Menzenschwand.

	vyacheslavite		(Ca, *REE*)-rich vyacheslavite		uraninite		
	n = 9	1σ	*n* = 3	1σ	*n* = 5	1σ	EPMA standard
SO_3	0.13	0.07	0.06	0.04	bdl		$SrSO_4$
P_2O_5	17.00	0.83	15.59	0.13	2.28	0.14	apatite
As_2O_5	1.56	0.06	0.85	0.15	3.91	0.08	lammerite
SiO_2	1.72	0.20	2.28	0.12	0.34	0.02	sanidine
UO_2	70.75	1.63	57.26	1.08	89.41	0.05	UO_2
Al_2O_3	0.34	0.03	0.15	0.02	0.48	0.04	sanidine
Y_2O_3	2.73	0.31	10.82	0.19	0.18	0.04	YAG
Sm_2O_3	0.12	0.06	0.23	0.07	bdl		$SmPO_4$
Eu_2O_3	bdl		0.11	0.03	bdl		$EuPO_4$
Gd_2O_3	0.30	0.06	0.64	0.11	bdl		$GdPO_4$
Tb_2O_3	bdl		0.18	0.02	bdl		$TbPO_4$
Dy_2O_3	0.41	0.06	1.13	0.05	bdl		$DyPO_4$
Ho_2O_3	0.09	0.07	0.36	0.14	bdl		$HoPO_4$
Er_2O_3	0.22	0.07	0.76	0.07	bdl		$ErPO_4$
Tm_2O_3	bdl		0.16	0.04	bdl		$TmPO_4$
Yb_2O_3	0.22	0.07	0.69	0.07	bdl		$YbPO_4$
CaO	0.82	0.14	3.72	0.07	0.34	0.03	apatite
FeO	0.06	0.05	0.04	0.03	0.06	0.02	hematite
PbO	bdl		bdl		0.23	0.02	vanadinite
Total	96.47		95.04		97.23		

bdl – below detection limits

Table 2. Average *REE* concentrations in uraninite and vyacheslavite from Menzenschwand obtained from the ICP-MS (in ppm).

	uraninite		vyacheslavite	
	$n = 6$	1σ	$n = 6$	1σ
Sc	82.4	3.22	161	54.5
Y	2108	231	25100	6429
La	7.86	1.39	9.7	3.04
Ce	68.5	7.17	163	47.2
Pr	26.8	1.65	89.7	26.1
Nd	235	5.89	897	258
Sm	211	3.4	1073	287
Eu	71.4	2.08	433	113
Gd	232	10.4	1926	519
Tb	64.2	1.86	486	123
Dy	450	14.6	3483	859
Ho	80.9	3.41	652	161
Er	238	9.9	2026	502
Tm	36.8	1.6	301	77
Yb	269	7.12	2199	567
Lu	30.1	1.56	301	80.5
∑*Ln*	2022		14039	

Table 3. Summary of the Ca occupancy in Ca- vyacheslavite $U_{1-x}Ca_xPO_4(OH)_{1-2x}(OH_2)_{2x}$ in the 4 crystals refined from 3D ED data independently and combined.

data	*Crystal 1*	*Crystal 2*	*Crystal 3*	*Crystal 4*	*combined*	*combined*
Nobs/Nall	1478/2440	2066/4414	1870/4217	1395/3537	6809/14608	6809/14608
R(obs)/wR(obs)	9.31/8.96 %	8.52/7.98 %	9.51/9.13 %	8.59/8.15 %	9.10/8.72 %	9.19/8.81 %
x	0.057(7)	0.104(5)	0.105(5)	0.123(5)	0.104(3)	0

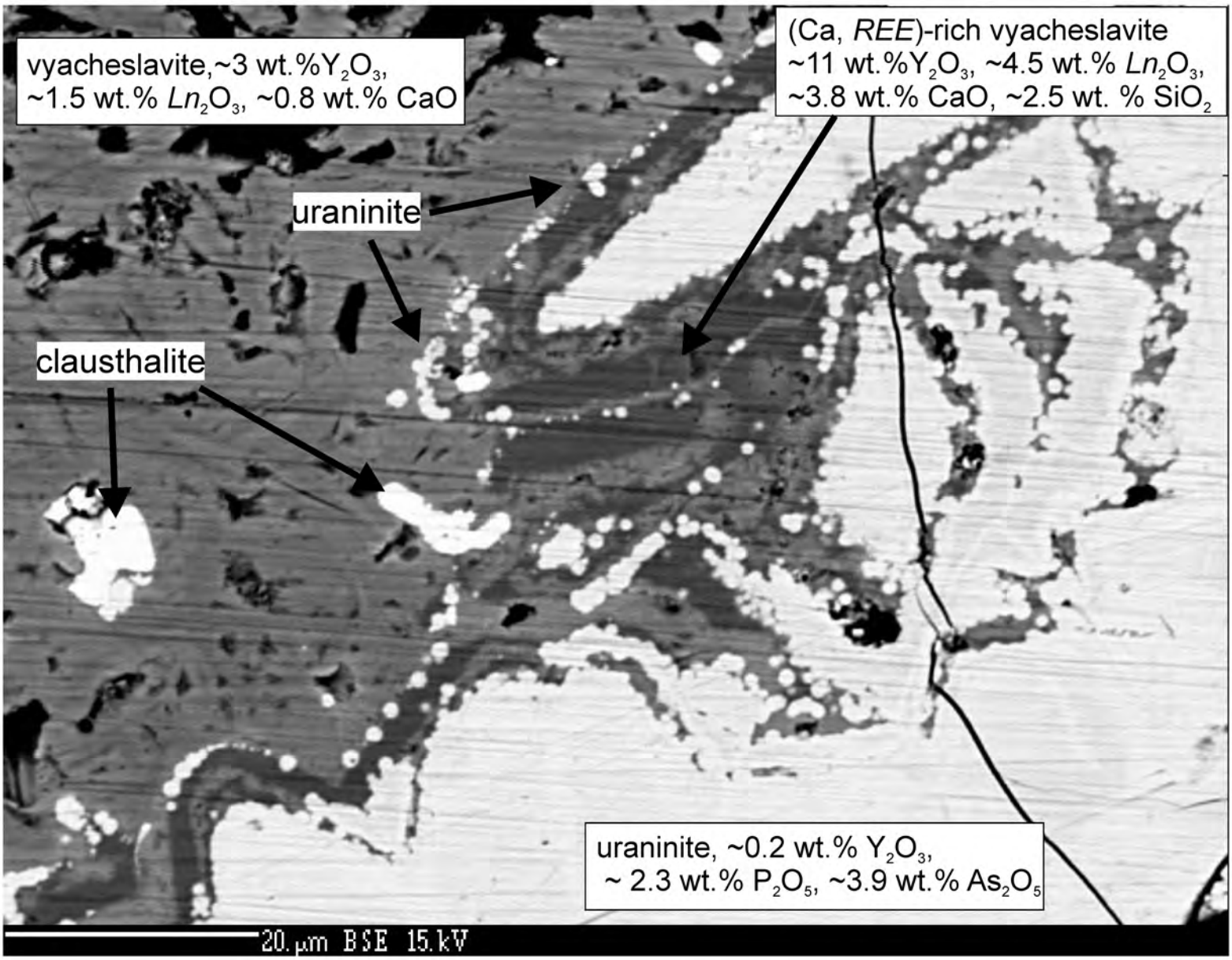
vyacheslavite,~3 wt.%Y_2O_3,
~1.5 wt.% Ln_2O_3, ~0.8 wt.% CaO
(Ca, *REE*)-rich vyacheslavite
~11 wt.%Y_2O_3, ~4.5 wt.% Ln_2O_3,
~3.8 wt.% CaO, ~2.5 wt. % SiO_2
uraninite
clausthalite
uraninite, ~0.2 wt.% Y_2O_3,
~ 2.3 wt.% P_2O_5, ~3.9 wt.% As_2O_5
20.μm BSE 15.kV

1

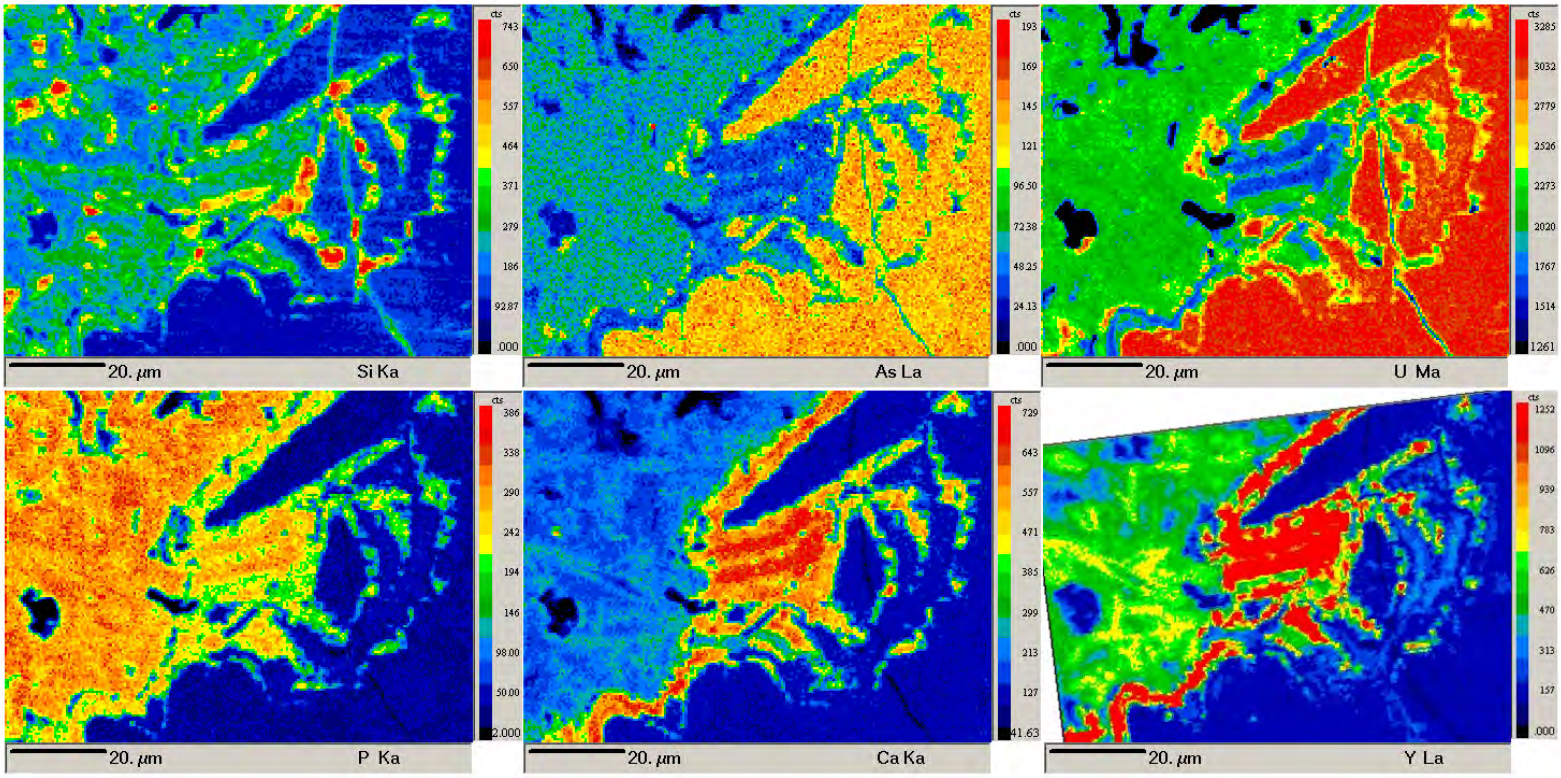
cts
743
650
557
464
371
279
186
92.87
.000
20. µm
Si Ka
cts
193
169
145
121
96.50
72.38
48.25
24.13
.000
20. µm
As La
cts
3285
3032
2779
2526
2273
2020
1767
1514
1261
20. µm
U Ma
cts
386
338
290
242
194
146
98.00
50.00
2.000
20. µm
P Ka
cts
729
643
557
471
385
299
213
127
41.63
20. µm
Ca Ka
cts
1252
1096
939
783
626
470
313
157
.000
20. µm
Y La

2

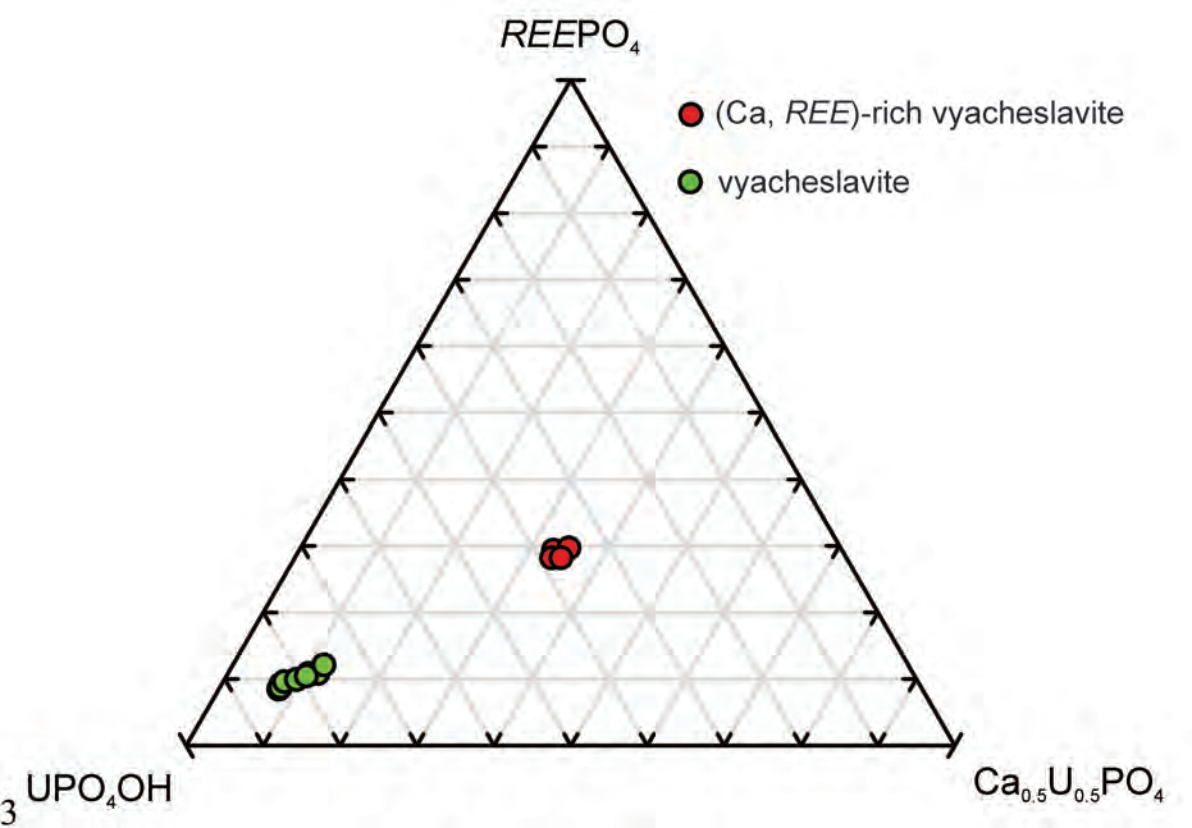
REEPO4
(Ca, REE)-rich vyacheslavite
vyacheslavite
UPO4OH
Ca0.5U0.5PO4

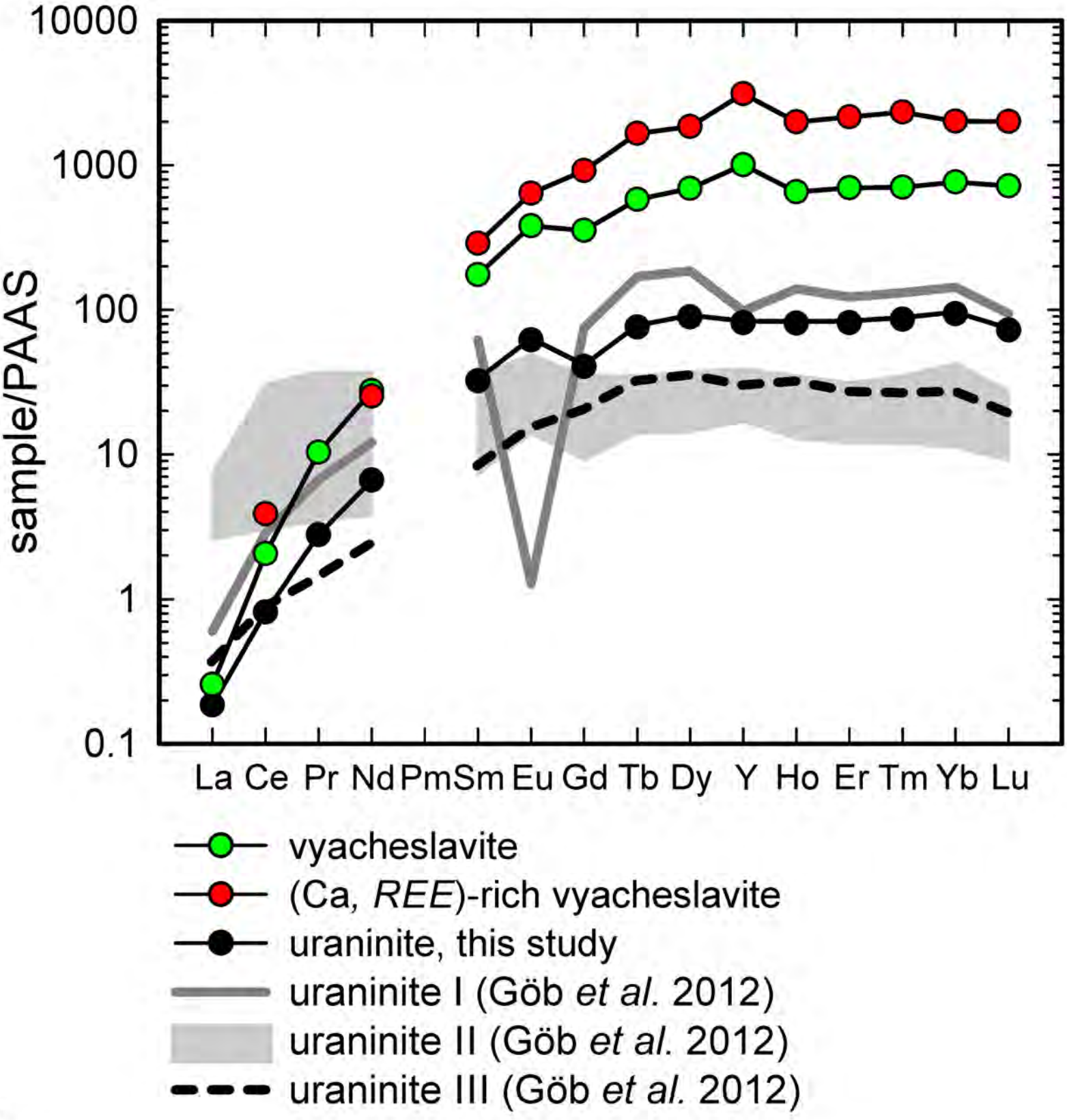
10000
1000
100
10
1
0.1
sample/PAAS
La Ce Pr Nd Pm Sm Eu Gd Tb Dy Y Ho Er Tm Yb Lu
vyacheslavite
(Ca, *REE*)-rich vyacheslavite
uraninite, this study
uraninite I (Göb *et al.* 2012)
uraninite II (Göb *et al.* 2012)
uraninite III (Göb *et al.* 2012)

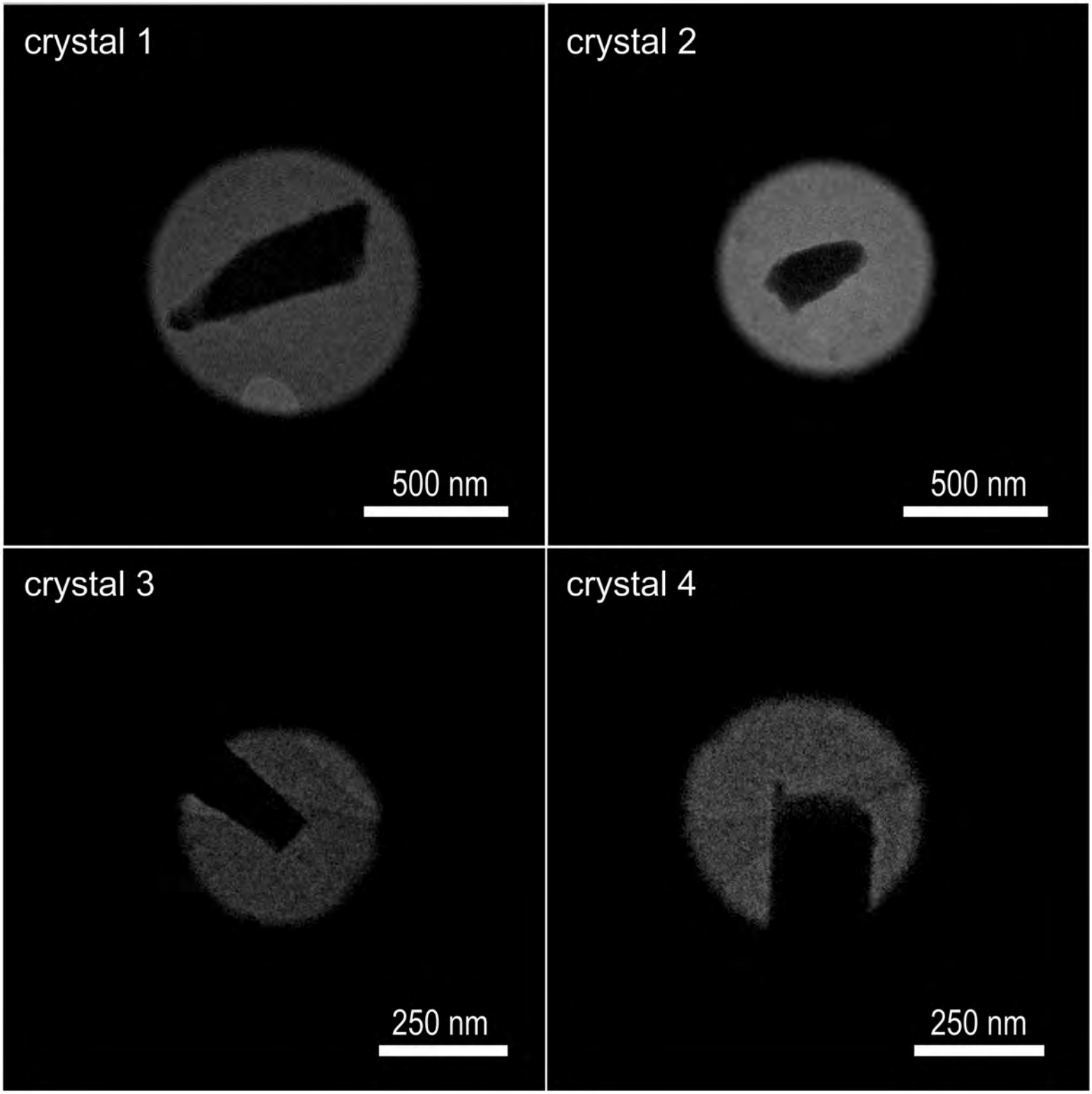
crystal 1
500 nm
crystal 2
500 nm
crystal 3
250 nm
crystal 4
250 nm

5

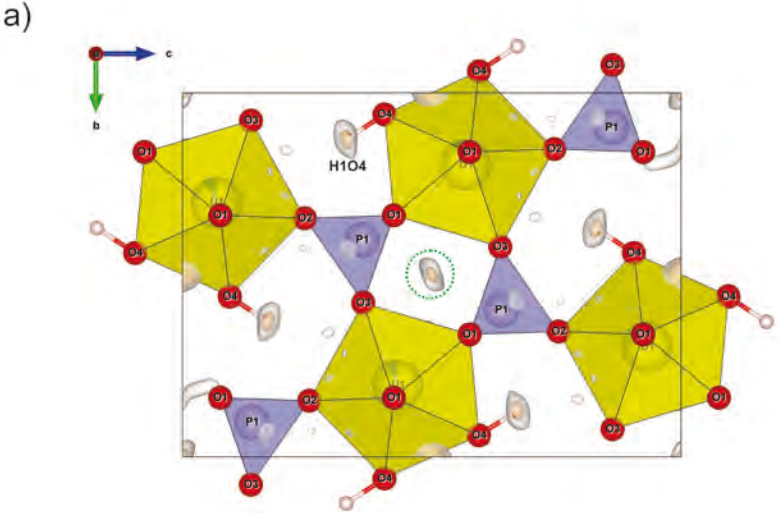
a)
c
b
H1O4
O1
O2
O3
O4
P1

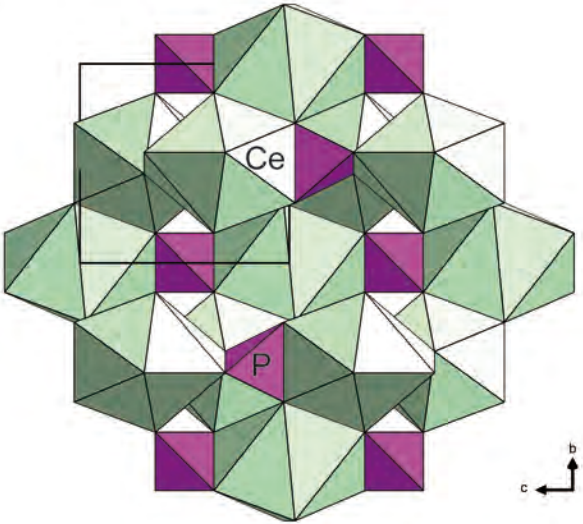
b)
Ce
P
b
c

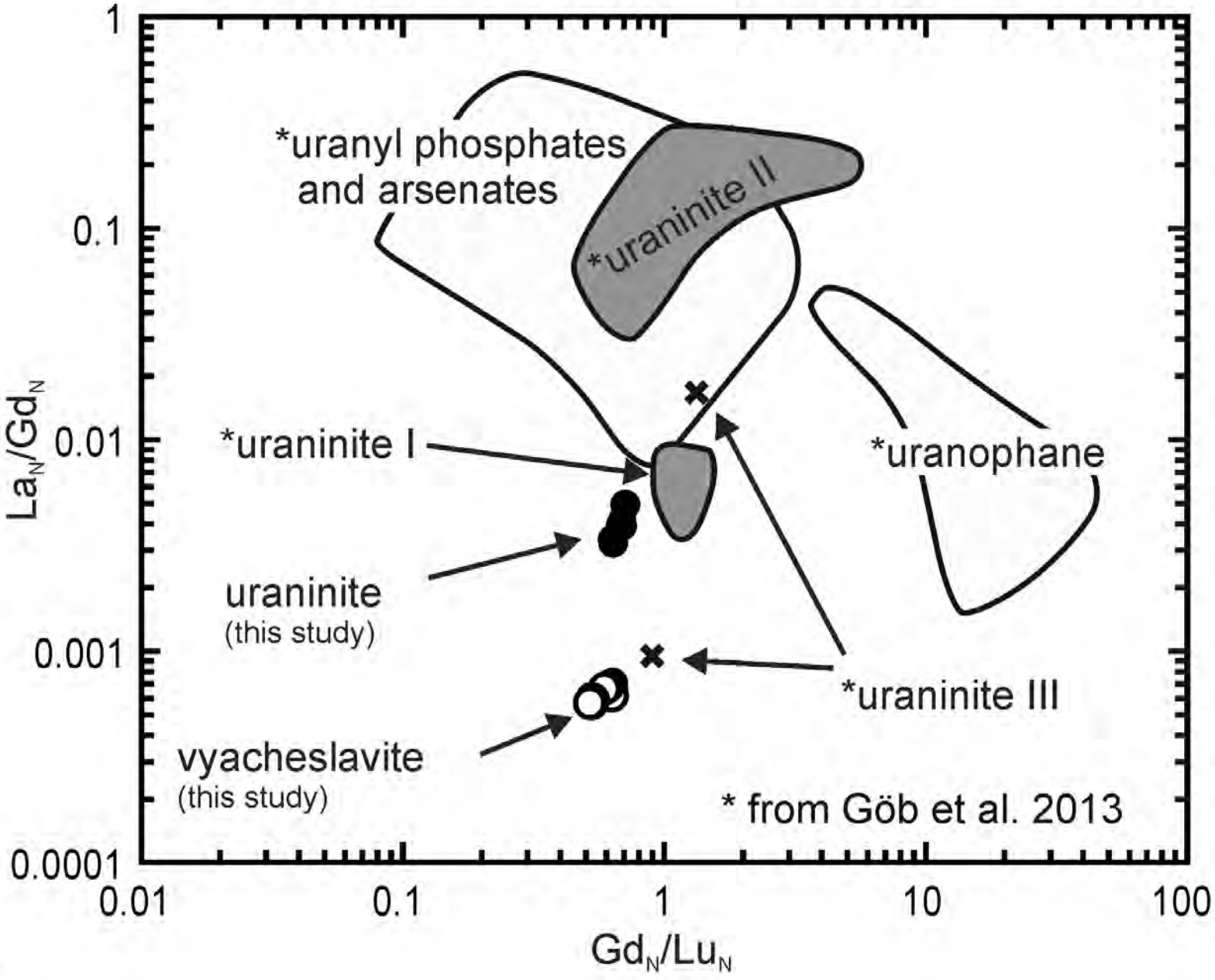
1
0.1
0.01
0.001
0.0001
0.01
0.1
1
10
100
La_N/Gd_N
Gd_N/Lu_N
*uranyl phosphates and arsenates
*uraninite II
*uraninite I
*uranophane
uraninite
(this study)
*uraninite III
vyacheslavite
(this study)
* from Göb et al. 2013

7